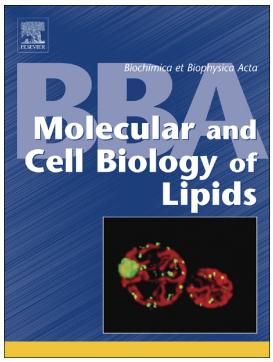

LAPTM4B controls the sphingolipid and ether lipid signature of small extracellular vesicles

Andrea Dichlberger, Kecheng Zhou, Nils Bäck, Thomas Nyholm, Anders Backman, Peter Mattjus, Elina Ikonen, Tomas Blom

PII: S1388-1981(20)30247-X

DOI: https://doi.org/10.1016/j.bbalip.2020.158855

Reference: BBAMCB 158855

To appear in: *BBA - Molecular and Cell Biology of Lipids*

Received date: 18 June 2020

Revised date: 3 November 2020

Accepted date: 5 November 2020

Please cite this article as: A. Dichlberger, K. Zhou, N. Bäck, et al., LAPTM4B controls the sphingolipid and ether lipid signature of small extracellular vesicles, *BBA - Molecular and Cell Biology of Lipids* (2020), https://doi.org/10.1016/j.bbalip.2020.158855

LAPTM4B controls the sphingolipid and ether lipid signature of small extracellular vesicles

Andrea Dichlberger[abe], Kecheng Zhou[ab], Nils Bäck[a], Thomas Nyholm[c], Anders Backman[c], Peter Mattjus[c], Elina Ikonen[ab], Tomas Blom[abd*]

[a] Department of Anatomy and Research Programs Unit, Faculty of Medicine, University of Helsinki, Helsinki, Finland
[b] Minerva Foundation Institute for Medical Research, Helsinki Finland
[c] Biochemistry, Faculty of Science and Engineering, Åbo Akademi University, Turku, Finland

*corresponding author:
Name: Tomas Blom
Email address: (tomas.blom@helsinki.fi)
Address: Faculty of Medicine, University of Helsinki, Haartmaninkatu 8, 00140, Finland

ORCIDs and email addresses

Andrea Dichlberger: 0000-0002-2083-3283, andrea.dichlberger@helsinki.fi

Kecheng Zhou: 0000-0003-1753-2524, kecheng.zhou@helsinki.fi

Nils Bäck: 0000-0001-9992-3726, nils.back@helsinki.fi

Thomas Nyholm: 0000-0002-1980-3693, thomas.nyholm@abo.fi

Anders Backman: 0000-0001-8144-4030, andersba@abo.fi

Peter Mattjus: 0000-0001-8991-5933, Peter.Mattjus@abo.fi

Elina Ikonen: 0000-0001-8382-1135, elina.ikonen@helsinki.fi

Tomas Blom: 0000-0001-9711-8287, tomas.blom@helsinki.fi

Footnote:
[d] Current address: Orion Corporation, Orion Pharma, Turku, Finland.
[e] Current address: Helsinki Innovation Services Ltd., Helsinki, Finland.

Highlights

- A sphingolipid interaction motif regulates LAPTM4B sorting in endosomes.
- LAPTM4B is secreted from cells via extracellular vesicles *in vitro* and *in vivo*.
- The glycosphingolipid and ether lipid signature of extracellular vesicles is regulated by LAPTM4B.
- LAPTM4B modulates nanodomain formation in extracellular vesicle membranes.

Abstract

Lysosome Associated Protein Transmembrane 4B (LAPTM4B) is a four-membrane spanning ceramide interacting protein that regulates mTORC1 signaling. Here, we show that LAPTM4B is sorted into intraluminal vesicles (ILVs) of multivesicular endosomes (MVEs) and released in small extracellular vesicles (sEVs) into conditioned cell culture medium and human urine. Efficient sorting of LAPTM4B into ILV membranes depends on its third transmembrane domain containing a sphingolipid interaction motif (SLim). Unbiased lipidomic analysis reveals a strong enrichment of glycosphingolipids in sEVs secreted from LAPTM4B knockout cells and from cells expressing a SLim-deficient LAPTM4B mutant. The altered sphingolipid profile is accompanied by a distinct SLim-dependent co-modulation of ether lipid species. The changes in the lipid composition of sEVs derived from LAPTM4B knockout cells is reflected by an increased stability of membrane nanodomains of sEVs. These results identify LAPTM4B as a determinant of the glycosphingolipid profile and membrane properties of sEVs.

Keywords: ether lipids, extracellular vesicles, exosomes, glycosphingolipids, membrane nanodomains, sphingolipids

Abbreviations: A4GATL, alpha-1,4-galactosyltransferase; B4GALT6, beta-1,4-galactosyltransferase; DES, desaturase; EV, extracellular vesicle; GBA, glucosylceramidase beta; GlcCer, glucosylceramide; GCS, glucosylceramide synthase; HexCer, hexosylceramide; ILV, intraluminal vesicle; KDSR, 3-ketosphinganine reductase; LacCer, lactosylceramide; LAPTM4B, Lysosome associated protein transmembrane 4B; MVE, multivesicular endosome; CERS1-6, ceramide synthases 1-6; SLim, sphingolipid interaction motif; SPT, serine palmitoyl-transferase.

1. Introduction

EVs are small membrane delimited particles that are released from cells and mediate intercellular communication. Lipids are key structural components involved in the formation and release of EVs [1,2]. EVs can also accommodate signaling lipids that contribute to their biological activity in recipient cells [3]. The most investigated types of EVs are exosomes that derive from late endosomal compartments. The formation of exosomes is initiated by inward budding of the delimiting endosomal membrane to generate multivesicular endosomes (MVEs) containing intraluminal vesicles (ILVs). MVEs that fuse with the plasma membrane release their internal vesicles as exosomes into the extracellular space [1]. The lipid composition of exosomes likely resembles that of the cellular compartment from which they originate, and is distinct from the cellular lipidome [1,4]. In particular, cholesterol (Chol), ceramide (Cer), sphingomyelin (SM), and phosphatidylserine (PS) are enriched in exosomal membranes [4,5]. However, the degree of enrichment varies between different cell types [4].

A critical step in the initial phase of ILV biogenesis is the sorting of molecular cargo, including lipids, in a controlled manner. This process is driven by multiple mechanisms. While it is widely accepted that the ESCRT (endosomal sorting complex required for transport) machinery is important for ILV formation, vesicles can also form in the absence of key ESCRT proteins [6]. These alternative mechanisms may be controlled by lipids, tetraspanins or heat shock proteins [7–11]. Lipid pathways linked to EV biogenesis include the generation of ceramide by neutral sphingomyelinase 2 (nSMase2), the formation of phosphatidic acid by phospholipase D2 (PLD2) [9,12] or hexadecyl-glycerol, the precursor of ether phospholipids [13]. Especially, nSMase2-mediated generation of ceramide was shown to trigger ILV budding into MVEs [9], but this mechanism can only be observed in certain cell systems [10,14–17]. The lipid-related mechanisms have been mostly studied in the context of regulating EV abundance, whereas factors controlling the EV lipid composition *per se* are unknown. The development of advanced analytical tools has broadened our knowledge regarding the lipid profile of EVs in recent years [4,5]. For example, shot-gun lipidomics has been utilized to identify unique EV lipid signatures as potential biomarkers of prostate cancer patients [18].

We recently showed that Lysosome associated protein transmembrane 4B (LAPTM4B) contains a functional sphingolipid interaction motif (SLim) in its third transmembrane domain [19,20]. Interestingly, LAPTM4B has been linked to poor prognosis in various types of cancers, and regulates mTORC1 signaling and autophagy [19,21–23]. Here, we show that sorting of LAPTM4B into ILVs of MVEs depends on its SLim. We provide the first evidence

that LAPTM4B is secreted from human cells in sEVs *in vitro* and *in vivo*. LAPTM4B regulates the glycosphingolipid and ether lipid composition of sEVs in a SLim-controlled manner, and modulates EV membrane properties.

2. Materials and Methods

2.1. Cell culture and cell treatments

The human epidermoid carcinoma cell line A431 (ATCC, Cat#CRL-1555) was maintained in Dulbecco's modified Eagle's medium containing 10% fetal bovine serum (FBS), penicillin/streptomycin (each 100 U/mL) and L-glutamine (2 mM) at 37°C in 5% CO_2. Plasmid transfections were carried out by X-tremeGENE HP DNA Transfection Reagent (Roche, Cat#06366546001) or Lipofectamine LTX with PLUS reagent (Invitrogen, Cat#15338030), according to the manufacturer's instructions. For enlargement of endosomal/lysosomal compartments, cells were treated with 1 μM Vacuolin-1 for 4 h at 37°C. All cell lines were tested negative for mycoplasma contamination using PCR.

2.2. Plasmids

LAPTM4B-24-3xFlag and mutant LAPTM4B-24-ATM3-3xFlag plasmids were generated as described previously [19,24]. LAMP1-mGFP was kindly provided by Esteban Dell'Angelica [25] (Addgene plasmid # 34831).

2.3. Generation of stable cell lines

LAPTM4B knockout A431 cells (designated name in this study: KO) were generated as described previously [19]. Briefly, A431 cells were co-transfected (using Lipofectamine) with Cas9 nickcase and two matching pairs of sgRNA-expressing plasmids. Transfected cells were subjected to puromycin selection for 48 h and subsequently cultured without selection for 4 additional days. Single clones were isolated and verified by sequencing. For the generation of endogenously-tagged LAPTM4B-sfGFP stable cells, superfold-GFP [26] and a 2XGGGGS linker were inserted at the C-terminus endogenous LAPTM4B by CRISPR/Cas9-mediated genome editing [27,28]. A homology-directed repair (HDR) template was generated by overlap PCR. A431 cells were co-transfected with the HDR template and a vector encoding Cas9, sgRNA targeting the C-terminal genomic locus of LAPTM4B, and a puromycin selection marker. Transfected cells were subjected to selection for 48 h, single clones were isolated, and verified by sequencing. For the generation of A431 stable cell lines expressing LAPTM4B-24 (short isoform of WT LAPTM4B; designated name in this study: L4B) or LAPTM4B-24-ATM3 (short isoform of LAPTM4B ceramide-binding deficient mutant; designated name in this study: ATM3) were described previously [19,24]. Briefly,

A431 LAPTM4B knockout cells (KO) were transfected with pEFIRES-P plasmids containing either L4B-3xFlag or ATM3-3xFlag and cells were subjected to puromycin selection (1 µg/mL) until a resistant cell pool was formed.

2.4. Immunofluorescence staining and confocal microscopy

Cells were seeded on glass coverslips 48 h prior to fixation. Cells were fixed with 4% paraformaldehyde in PBS for 20 min at room temperature, quenched with 50 mM NH_4Cl for 10 min at room temperature, permeabilized with 0.1% Triton X-100 in PBS for 5 min at room temperature, blocked with 10% fetal bovine serum in PBS for 30 min at 37°C and subsequently probed with primary antibodies (Anti-GFP, 1:5,000 (ab290, Abcam); anti-CD63, 1:200 (BD556019, clone H5C6, BD Biosciences), anti-LAMP1, 1:400 (sc-20011,Clone H4A3, SCBT); anti-LBPA 1:1,000 (#MABT837, clone 6C4, Sigma)) for 45 min at 37°C. Cells were washed with PBS and labeled with secondary antibodies accordingly. Finally, cell nuclei were counterstained with DAPI, coverslips were rinsed in MQ H_2O and mounted on microscope slides using Mowiol/DABCO (Calbiochem, Cat#475904/ Sigma, Cat#D-2522). Images were captured with a Leica TCS SP8X microscope.

To quantify the amount of L4B or ATM3 within the delimiting membrane of Vacuolin-1-enlarged endosomes, z-sections of individual endosomes were taken. LAMP1-mGFP was used as delimiting membrane marker and reference to obtain the central z-section of an endosome image stack. In addition, the LAMP1-mGFP-positive central z-section of each endosome was used to measure the diameter of the endosome. Fluorescence intensities of the proteins of interest were quantified within endosome lumen (area inside the delimiting membrane) and in the delimiting membrane using Image J (version 1.50b).

2.5. Immunoelectron microscopy

For electron microscopical immunolabeling, stable cell lines (L4B and ATM3) were fixed with 2% formaldehyde, 0.01 M periodate and 0.075 M lysine-HCl in 0.075 M phosphate buffer for 2 h at room temperature [29], permeabilized with 0.01% saponin for 8 min, labeled with anti-DDDK tag antibody (Abcam, ab21536; 1:50 dilution) for 1 h, then incubated with 1.4 nm diameter nano-gold-conjugated Fab fragments against rabbit immunoglobulin G (Nanoprobes; 1:60 dilution) for 1 h, post-fixed with 1% glutaraldehyde and quenched with 50 nM glycine. Nano-gold particles were then intensified using the HQ Silver Enhancement kit (Nanoprobes, cat.no. 2012) followed by gold toning in subsequent incubations in 2% sodium acetate, 0.05% $HAuCl_4$ and 0.3% $Na_2S_2O_3 \cdot 5H_2O$ [30]. After washing, the cells were processed for Epon embedding. Ultrathin sections were cut parallel to the coverslip, post-stained with uranyl acetate and lead citrate and systematically photographed at 15000X with a Jeol JEM-1400 electron microscope equipped with a Gatan Orius SC 1000B bottom

mounted CCD camera to give a total of 30 multivesicular bodies for each specimen. The results from 2 separate experiments yielding about 900 ILVs/cell type were analyzed. For analyzing the ILV position within the MVE lumen in Figure 1D, MVEs with a minimum of 6 gold labeled ILVs were quantified.

2.6. Isolation of EVs

The isolation of EVs from cell culture-conditioned medium was carried out with modifications as described previously [31–34]. The EV release and isolation protocol, used in this study, has been optimized for A431 cells as follows. Cells were seeded in complete cell culture medium (70% confluency). After 24 h, cells were washed 3 times with PBS and subsequently cultured for another 48 h in serum-free medium to obtain EV-conditioned medium. The entire 48 h-EV-conditioned medium was collected and centrifuged at 300 x g for 10 min and 2,500 x g for 25 min at 4°C to remove cell debris and apoptotic bodies. All ultracentrifugation steps were carried out in either a Beckman Optima LE-80K ultracentrifuge or a table top OptimaMAX ultracentrifuge. The supernatant was transferred to polycarbonate centrifuge bottles (Beckman Coulter Cat#355618) and centrifuged at 10,000 x g for 40 min at 4°C using a Type 70Ti rotor (fixed-angle) to obtain a 10K microvesicle-enriched EV population (designated as large EV; lEV). The resulting supernatant was transferred to fresh centrifuge bottles and ultracentrifuged at 110,000 x g for 2 h at 4°C using a 70Ti rotor to obtain a 110K exosome-enriched EV population (designates as small EV; sEV). Both, lEV and sEV pellets have been resuspended in DPBS, transferred to small polycarbonate centrifuge tubes (Beckman, Cat#343622) and re-pelleted by ultracentrifugation at 10,000 x g for 22 min (lEV) and 110,000 x g for 40 min (sEV) at 4°C using a TLA100.3 rotor. Final EV pellets were carefully resuspended in DPBS, transferred to low-binding 1.5 mL tubes, snap-frozen in liquid nitrogen, and stored at -80°C. For control samples, the serum-free medium was subjected to the entire EV isolation procedure.

2.7. Transmission electron microscopy of EVs

EVs were prepared for electron microscopy as described previously [35]. Briefly, EVs were loaded on carbon- and pioloform-coated glow discharged copper grids (mesh 200). Samples were fixed with 2% PFA in 0.1 M $NaPO_4$ buffer (pH 7.0), stained with 2% neutral uranyl acetate and embedded in a uranyl acetate/methylcellulose mixture (1.8/0.4%). EVs were viewed by transmission EM using Jeol JEM-1400 (Jeol Ltd., Tokyo, Japan) operating at 80kV. Images were taken with a Gatan Orius SC 1000B CCD-camera (Gatan Inc., USA) with 4008 x 2672 px image size and no binning.

2.8. Nanoparticle tracking analysis

The concentration and size distributions of EVs were measured by nanoparticle tracking

analysis (NTA) using a LM14 view unit (Malvern Instruments Ltd, Malvern, UK) equipped with a blue laser (405 nm, 70mW) and a sCMOS camera (Hamamatsu Photonics, Hamamatsu, Japan). Each EV replicate sample was measured under constant equipment settings using camera level 14. 5 videos each 90 sec acquisition time were recorded for each replicate. All data were recorded and analyzed using NanoSight software version NTA 3.0 (NanoSight, Amesbury, UK).

2.9. Precipitation of secreted proteins

Secreted proteins were precipitated by using tricholoracetic acid (TCA) from serum-free EV-conditioned media as follows. Equal volumes of EV-conditioned medium were incubated with 0.02% sodium dexoycholate for 15 min at room temperature. Samples were subsequently incubated with 15% trichloroacetic acid for 1 h at 4°C. Precipitated proteins were pelleted by centrifugation for 10 min at 16,000 x g at 4°C and washed once with ice-cold acetone. Finally, precipitated protein pellets were air-dried, and resuspended in 1x non-reducing sample loading buffer.

2.10. Western blotting

Cells were washed with PBS and lysed with ice-cold lysis buffer (50 mM HEPES, 25 mM NaCl, 5 mM EDTA, 1% NP-40, pH 7.4) containing protease inhibitor cocktail (Sigma, Cat#I3786). Cell lysates were cleared by centrifugation at 16,000 x g for 10 min at 4°C. For Western blotting of EVs, EV pellets of lEV or sEV fractions were directly lysed in equal volumes of lysis buffer. Equal amounts of EVs isolated from equal input volumes of culture-conditioned medium or equal volumes (of initial media input) of TCA-precipitated proteins were resolved by 12% Mini-Protein TGX Stain-Free gels (BioRad Cat#161-0185) and transferred onto LF-PVDF membrane (BioRad, Cat#170-4274). Membranes were blocked with 5% milk in TBS containing 0.1% Tween-20 for 1 h at room temperature, and subsequently probed with primary antibodies (Anti-LAPTM4B, Atlas Antibodies, Cat#AMAb91356 1:1000; anti-Flag M2, Sigma-Aldrich, Cat#F1804, 1:2000; anti-CD63, 1:1000 (BD556019, clone H5C6, BD Biosciences); anti-CD81, 1:1000 (sc-23962, clone 5A6, SCBT); anti-GAPDH, 1:10 000 (G9545, Sigma) over night at 4°C. After washing with TBS 0.1% Tween-20, membranes were incubated with HRP-conjugated secondary antibodies for 45 min at room temperature. Finally, membranes were washed, incubated with ECL Clarity (BioRad, Cat#170-5060) or ECL Clarity Max substrate (BioRad, Cat#170-5062), and imaged with a ChemiDoc MP Imgang System (BioRad). Band intensities were analyzed using Image Lab software (version 6.0; BioRad) or Image J software (version 1.50b; https://imagej.nih.gov/ij/) and normalized to total protein content quantified with Stain-Free technology (BioRad).

2.11. Lipidomic analysis of cells and EVs by ESI-MS/MS

Mass spectrometry-based lipid analysis was performed by Lipotype GmbH (Dresden, Germany) as described [36]. Lipidomes were generated from cells (3-4 replicates) under serum-free conditions and their corresponding secreted lEV (2-3 replicates) and sEV (2-3 replicates) populations of WT, KO, L4B, and ATM3 cell lines. The following lipid nomenclature has been used in this study. Lipid categories including GL, glycerolipids; GP, glycerophospholipids; LGP, lyso-glycerophospholipids; SL; sphingolipids; and ST, sterols. Lipid classes including CE, cholesterol ester; Cer, ceramide; Chol, cholesterol; CL; DG, diacylglycerol; HexCer, hexosylceramide; PA, phosphatidic acid; PC, phosphatidylcholine; PE, phosphatidylethanolamine; PG, phosphatidylglycerol; PI, phosphatidylinositol; PS, phosphatidylserine; and their respective lysospecies LPA; LPC; LPE; LPG; LPI; LPS; and their ether derivates: PC O-; LPC O-; PE O-; LPE O-; SM, sphingomyelin; TG, triacylglycerol. The glycosphingolipids glucosylceramides (GlcCer) and galactosylceramides (GalCer) are grouped as hexosylceramides (HexCer). Lipid species were annotated as follows (exemplified for SL species): [sum of hydroxyl groups in the long chain base and the fatty acid moiety; m, mono; d, di; t, tri] [lipid class] [sum of carbon atoms in the long chain base and the fatty acid moiety]:[sum of double bonds in the long chain base and the fatty acid moiety]; (for example: Cer(d34:1)). Note that mono(m)-sphingolipid species represent deoxysphingolipids. If available, individual fatty acid composition following the same annotation is given in brackets (for example: (18:1;0_24:2;0). For lipid extraction, lipids were extracted using a two-step chloroform/methanol procedure [37]. Samples were spiked with internal lipid standard mixture containing: CL(16:1_15:0_15:0_15:0); Cer(18:1;2_17:0); DG(17:0_17:0); HexCer(d18:1_12:0); LPA, lyso-phosphatidate 17:0; LPC, 12:0; LPE, 17:1; LPG, 17:1; LPI, 17:1; LPS, 17:1, PA(17:0_17:0); PC(17:0_17:0); PE(17:0_17:0); PG(17:0_17:0); PI(16:0_16:0); PS(17:0_17:0); CE, 20:0; SM(d18:1_12:0;0); TG(17:0_17:0_17:0) and Chol. After extraction, the organic phase was transferred to an infusion plate and dried in a speed vacuum concentrator. First-step dry extract was resuspended in 7.5 mM ammonium acetate in chloroform/methanol/propanol (1:2:4, V:V:V) and second-step dry extract in 33% ethanol solution of methylamine in chloroform/methanol (0.003:5:1; V:V:V). All liquid handling steps were performed using Hamilton Robotics STARlet robotic platform with the Anti Droplet Control feature for organic solvents pipetting. MS data acquisition. Samples were analyzed by direct infusion on a QExactive mass spectrometer (Thermo Scientific) equipped with a TriVersa NanoMate ion source (Advion Biosciences). Samples were analyzed in both positive and negative ion modes with a resolution of Rm/z=200=280000 for MS and Rm/z=200=17500 for MSMS experiments, in a single acquisition. MSMS was triggered by an inclusion list encompassing corresponding

MS mass ranges scanned in 1 Da increments [38]. Both MS and MSMS data were combined to monitor CE, DG and TG ions as ammonium adducts; PC, PC O-, as acetate adducts; and CL, PA, PE, PE O-, PG, PI and PS as deprotonated anions. MS only was used to monitor LPA, LPE, LPE O-, LPI and LPS as deprotonated anions; Cer, HexCer, SM, LPC and LPC O- as acetate adducts and cholesterol as ammonium adduct of an acetylated derivative [39]. Data analysis and post-processing. Data were analyzed with in-house developed lipid identification software based on LipidXplorer [36,40]. Data post-processing and normalization were performed using an in-house developed data management system. Only lipid identifications with a signal-to-noise ratio >5, and a signal intensity 5-fold higher than in corresponding blank samples were considered for further data analysis.

2.12. Time-resolved fluorescence analysis of EV membrane order

The *trans*-parinaric acid (tPA) was synthesized as described [41], and purified by crystallization from hexane [42]. It was stored at - 87°C and contained 1 mol% butylated hydroxytoluene to prevent oxidation. The properties of the sEVs were probed by measuring the emission lifetime of tPA. The stability of the tPA excited state is very sensitive to the order of its local environment [42–44]; hence, its emission lifetime varies in fluid and highly ordered membrane domains [45,46]. For this an amount of tPA estimated to be 1 mol% of the total lipid in the sEVs was placed in a glass vial, after which the solvent (ethanol) was evaporated at 40^{o}C under a constant flow of nitrogen. The collected sEVs were then applied on top of the dry tPA and incubated 0 5 h on ice. The samples were then diluted to give a final volume of 300 µL and a final lipid concentration around 13 µM. A FluoTime 100 spectrofluorometer with a TimeHarp260 pico time-correlated single-photon-counting module (PicoQuant, Berlin, Germany) was used for measurements. The tPA was excited with a 297 ± 10 nm LED laser source (PLS300, PicoQuant), and the emission was collected through a 435/40 nm single-band pass filter. Fluorescence decays were recorded at temperatures between ~5 and ~45^{o}C. The exact temperature of each measurement was checked with a thermometer in the cuvette. Data were analyzed using FluoFit Pro software obtained from PicoQuant.

2.13. Globotriaosylceramide (Gb3) labeling by STxB

Cells seeded on coverslips were transfected with siRNA Ctrl (Ambion, Cat#4390844), LAPTM4B (Ambion, Cat#s30811), or LAPTM4A (Ambion, Cat#s18791) for 72 h. The cells were washed in PBS, and labeled with 5 µg/ml STxB-Cy3 (kindly provided by Prof. Ludger Johannes, Institut Curie, Paris) for 15 min. After three washes with PBS, the cells were fixed with 4% PFA for 15 min. The cells were washed 3 times with PBS and incubated for 10 min

with 50 nM NH_4Cl. The coverslips were briefly rinsed with MQ H_2O and mounted on microscopy slides before imaging with a Leica TCS SP8X confocal microscope.

2.14. Glycosphingolipid synthesis assay

$3x10^6$ wild type (WT) and LAPTM4B knockout (KO) A431 cells were seeded in quadruplicate in complete medium in 10 cm dish 48 h prior to the [^{3}H]-sphingosine pulse. The cells were incubated with [^{3}H]-sphingosine (final concentration 1 µCi/ml) in serum-free DMEM containing 0.2% fatty acid free BSA (Sigma, Cat#A3803) for 120 min. The dishes were then washed twice with PBS and once with MQ H_2O, and air dried at room temperature. The lipids were extracted from the dishes and loaded on HPTLC plates for analysis as described previously [47]. Complex glycolipids were separated using a elution buffer containing chloroform:methanol:acetic acid:water to a ratio of 25:20:4:1. Simple glycolipids were separated using an elution buffer containing chloroform:methanol:acetone:acetic acid:water to a ratio of 10:2:4:2:1. All components of the elution buffers were HPLC-grade chemicals. After separation of the radioactively labeled lipids on the HPTLC plates, the plates were thoroughly dried and then placed against a BAS-TR imaging plate for 2 weeks or labeled with orcinol to visualize the labeled lipids. The resulting bands were then scanned and analyzed by ImageJ.

2.15. Statistical analysis of data

Data are presented as the mean ± standard error of mean (SEM) from at least three independent experiments. Statistical significance was calculated using the Student's t-test for pairwise comparisons or Chi-square test. The level of statistical significance was set at 0.05. * $p \leq 0.05$; ** $p \leq 0.005$; *** $p < 0.0005$.

3. Results

3.1. LAPTM4B sorting into intraluminal vesicles is controlled by its sphingolipid interaction motif

We set out to gain a deeper understanding of how the sphingolipid interaction motif (SLim) of LAPTM4B modulates organellar sphingolipid homeostasis. We first determined the subcellular localization of endogenous LAPTM4B in epidermoid carcinoma A431 cells used in our previous studies [19,21]. LAPTM4B was C-terminally tagged at the genomic locus with a superfold green fluorescent protein (sfGFP) by CRISPR/Cas9-mediated homology-directed repair. LAPTM4B-sfGFP was observed in punctate endosomal structures in the perinuclear area of the cell (**Fig. 1A, Supp. Fig. 1A**) and colocalized with

lysobisphosphatidic acid (LBPA), a negatively charged endosomal lipid involved in the formation of ILVs destined for secretion as exosomes [48]. Surprisingly, despite being classified as a lysosomal protein [49], endogenous LAPTM4B-sfGFP showed only partial overlap with the lysosomal marker LAMP1 (**Fig. 1A**). However, in agreement with previous studies [50,51], the overexpressed LAPTM4B and the SLim deficient mutant showed good colocalization with the late endosomal / lysosomal markers, including LAMP1 (**Supp. Fig. 1B**).

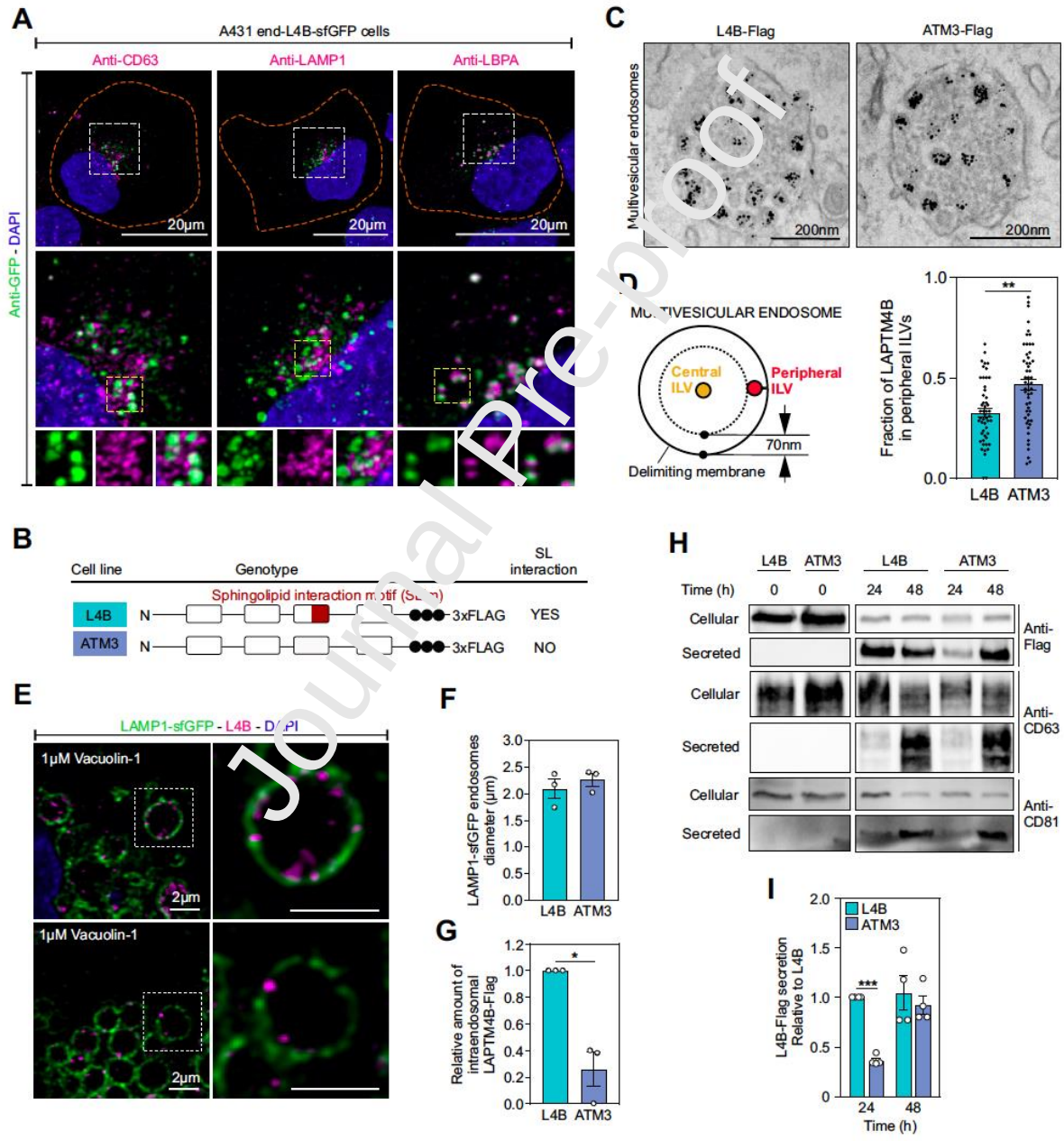

Fig. 1. LAPTM4B sorting into ILVs is controlled by a sphingolipid interaction motif (SLim). (A) Cellular localization of endogenously sfGFP-tagged LAPTM4B with CD63 (Pearson's Corr. 0.39 ± 0.04), LAMP1 (Pearson's Corr. 0.23 ± 0.03), and LBPA (Pearson's Corr. 0.45 ± 0.05) in A431 cells. (B) Schematic picture of cell lines stably expressing 3xFlag-

tagged WT (L4B) or SLim-deficient LAPTM4B (ATM3) in a LAPTM4B knockout background in A431 cells. (C) Representative electron microscopy images of immunogold-labeled L4B-Flag and ATM3-Flag cells. (D) Left panel: Schematic drawing depicting the criteria set for quantifying L4B- and ATM3-positive ILVs in proximity to the delimiting membrane of MVE. Right panel: ATM3-positive ILVs where more frequently found in the peripheral zone compared to L4B-positive ILVs. Each dot in the graph represents one quantified MVE. (E) Representative images showing the localization of L4B-Flag or ATM3-Flag within the lumen of vacuolin-1-enlarged endosomes. LAMP1-sfGFP defines the delimiting membrane. (F) Vacuolin-1-enlarged LAMP1-sfGFP-positive endosomes sizes (diameter in µm) in L4B and ATM3 cells (n = 3 independent experiments, mean ± SEM). (G) Quantification of (E) L4B-Flag or ATM3-Flag within the lumen of vacuolin-1-enlarged LAMP1-sfGFP-positive endosomes (n = 3 independent experiments, mean ± SEM, total number of analyzed endosomes: L4B (n=136), ATM3 (n=145). (H) Secreted L4B, ATM3, CD63 and CD81 were quantified by Western blotting of TCA-precipitated 24 h- and 48 h conditioned media. A representative image of cellular and secreted proteins is shown. (I) Quantification of secreted L4B and ATM3 shown in (H) (n = 3 independent experiments; mean ± SEM). *p≤ 0.05; ***p≤0.0005.

Next, we utilized immuno-EM to investigate whether SLim regulates the localization of LAPTM4B in multivesicular endosomes (MVEs). To this end, we re-expressed wild-type LAPTM4B (L4B) or SLim-deficient mutant LAPTM4B (ATM3) on a LAPTM4B knockout background (**Fig. 1B, Supp. Fig. 1B-D**) [19]. L4B was mainly found in ILVs of MVEs (**Fig. 1C**). L4B and ATM3 cells had similar amounts of ILVs per MVE, and number of gold labeled structures per MVE (**Supp. Fig. 2A**). As ceramide has been reported to play a role in ILV budding [9], we measured whether the SLim in LAPTM4B affects its localization in MVEs. L4B- and ATM3-positive ILVs were classified according to their position within the MVE lumen as either central ILVs or peripheral ILVs (**Fig. 1C – D, Supp. Fig. 2B**). The cut-off for peripheral ILVs was set to a distance of <70 nm from the MVE delimiting membrane, with the rationale that a budding ILV may still be continuous with the delimiting membrane within this distance. Remarkably, ATM3-positive ILVs were more frequently found in close proximity to the delimiting membrane compared to L4B-positive ILVs (**Fig. 1D, Supp. Fig. 2A**). To further address whether SLim regulates the sorting of LAPTM4B into ILVs, we assessed L4B and ATM3 localization in endosomal compartments enlarged by treatment with Vacuolin-1, a triazine derivative that promotes fusion of acidic organelles and inhibits calcium dependent lysosomal exocytosis [52] (**Fig. 1E – G, Supp. Fig. 2C**). LAMP1-sfGFP was expressed to mark the delimiting membrane of late endosomes [25]. The LAMP1-sfGFP organelles were of similar size in L4B and ATM3 expressing cells after treatment with Vacuolin-1 (**Fig. 1F**). Strikingly, there was ~75% less ATM3 in LAMP1-sfGFP-positive endosomes compared to WT L4B (**Fig. 1G)**, suggesting that the SLim regulates L4B localization in the MVE lumen. In addition, ATM3 had a higher tendency to localize at the

delimiting membrane compared to L4B (**Supp. Fig. 2D**).

3.2. LAPTM4B is secreted from cells

As ILVs can be secreted from cells in the form of exosomes, we tested whether the reduced sorting of ATM3 into ILVs is also reflected by its release from cells. Therefore, the amount of L4B and ATM3 was quantified from 24 h and 48 h conditioned cell culture medium. At the 24 h time point, ATM3 secretion was ~60% lower than that of L4B (**Fig. 1H - I)**, while similar amounts of L4B and ATM3 were detected in the medium at 48 h, suggesting that SLim affects L4B secretion dynamics. The mechanism behind the diminished L4B secretion after 24 h is not known, but may be related to its high turnover and downregulation under starvation conditions [53]. In contrast, secretion of the established exosome markers CD63 and CD81 [54], was similar from L4B and ATM3 expressing cells at both time points (**Fig. 1H - I**). Together, these data suggest that the efficient sorting of LAPTM4B into ILVs and the rapid release into the medium is facilitated by a functional SLim.

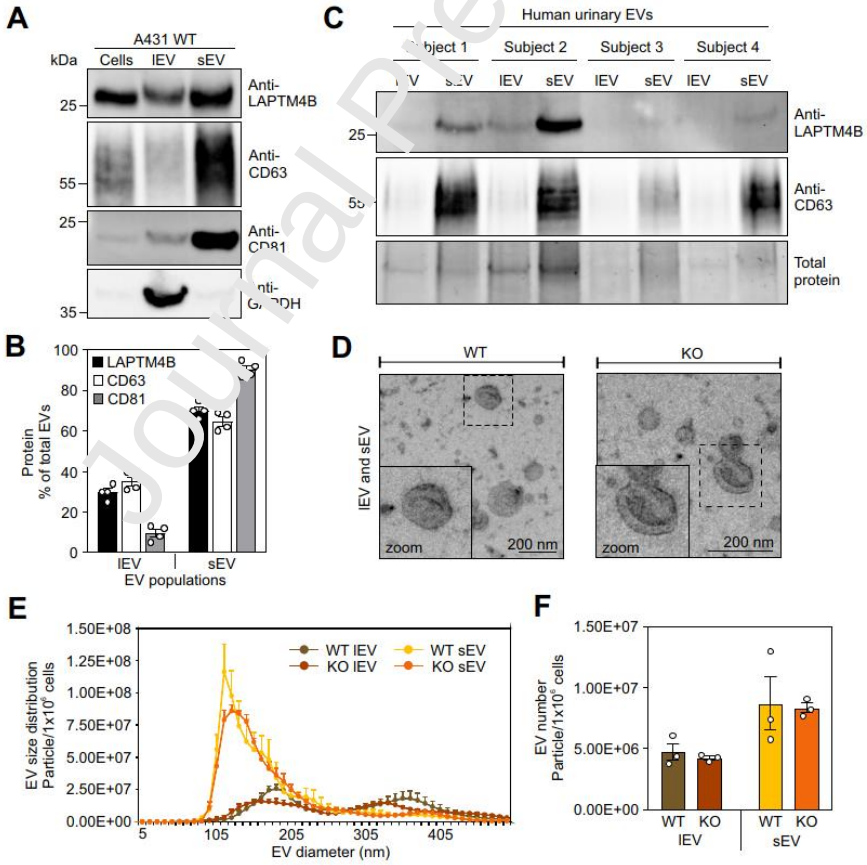

Fig. 2. LAPTM4B associates with small EVs in *vitro* and in *vivo*. (A) Large (lEV) and small (sEV) extracellular vesicle populations were isolated from serum-free 48 h conditioned medium by sequential ultracentrifugation. A representative image of a quantitative Western

blot analysis of endogenous LAPTM4B, CD63, CD81 and GAPDH in lEV and sEV populations and cells is shown. (B) Quantification of LAPTM4B, CD63 and CD81 protein distribution in lEV and sEV populations (n ≥ 3 independent experiments; mean ± SEM). (C) lEV and sEV populations were isolated from human urine of 4 different healthy subjects. Quantitative Western blot of LAPTM4B and CD63 in lEVs and sEVs is shown. (D) Representative transmission electron micrographs of lEVs and sEVs isolated from 48 h-conditioned medium of WT and KO cells are shown. Scale bar = 200 nm. (E) Size distribution of WT and KO lEVs and sEVs was determined by NTA (n = 3 independent experiments; mean ± SEM). (F) Particle number of WT and KO lEVs and sEVs was measured by NTA (n = 3 independent experiments; mean ± SEM).

3.3. LAPTM4B associates with small EVs

Considering that LAPTM4B localized to ILVs and was secreted from cells, we further tested whether LAPTM4B associates with certain types of EVs. EVs were isolated from 48 h-conditioned medium of A431 WT cells (**Fig. 2 A - B**) and human prostate cancer PC-3 cells (**Supp. Fig. 3A - B**) by sequential ultracentrifugation. This isolation method allowed us to separate two major EV categories, large EVs (lEV) enriched in microvesicles and small EVs (sEV) containing exosomes [31]. The majority of secreted LAPTM4B was detected in the sEV population in both cell lines, together with CD63 and CD81 [54] (**Fig. 2A - B; Supp. Fig. 3A - B**). Importantly, LAPTM4B also associated with sEVs isolated from urine of healthy human subjects (**Fig. 2C, Supp. Fig. 3C**). This is the first observation to demonstrate that LAPTM4B associates with EVs likely representing classical exosomes that originate from endosomal compartments. We next assessed whether LAPTM4B affects EV properties. Transmission-EM demonstrated that EV preparations contained characteristic cup-shaped vesicles, and that KO-derived EVs were morphologically similar to WT EVs (**Fig. 2D**). Nanoparticle tracking revealed that LAPTM4B depletion (**Fig. 2E - F**) or expression of mutant ATM3 (**Supp. Fig. 3D - F**) did not significantly affect the number or size distribution of the secreted EVs.

3.4. LAPTM4B differentially modulates the lipid composition of sEVs and their parental cells

Lipids are major constituents of EVs and have a substantial effect on the biophysical properties of membranes. To gain further insight into whether LAPTM4B controls lipid homeostasis, we performed lipidomic analysis of isolated sEVs and their parental A431 cells (**Supp. table 1 and 2**). Altogether, the lipid composition of WT, KO, rescue L4B, and mutant ATM3 cells and sEVs was analyzed. Principal component analysis (PCA) of cellular lipidomes showed a clear separation of WT and L4B rescue cells from KO and ATM3 cells (**Fig. 3A**). A total of 671 and 736 lipid species were identified in WT and KO cells, respectively (**Fig. 3B**). Similarly as in cells, the lipidomes of sEVs deriving from WT and KO cells were clearly separated in the PCA plot (**Fig. 3C**), and 610 lipid species were detected in WT sEVs compared to 614 in KO sEVs **(Fig. 3D**). Taken together, the total amount of

detected lipid species were similar in samples derived from WT, KO, L4B and ATM3 cells (**Supp. Fig. 4A - E**). However, the PCA results suggest that there are specific LAPTM4B-regulated lipids in cells and EVs, and that these effects are dependent on the SLim of LAPTM4B.

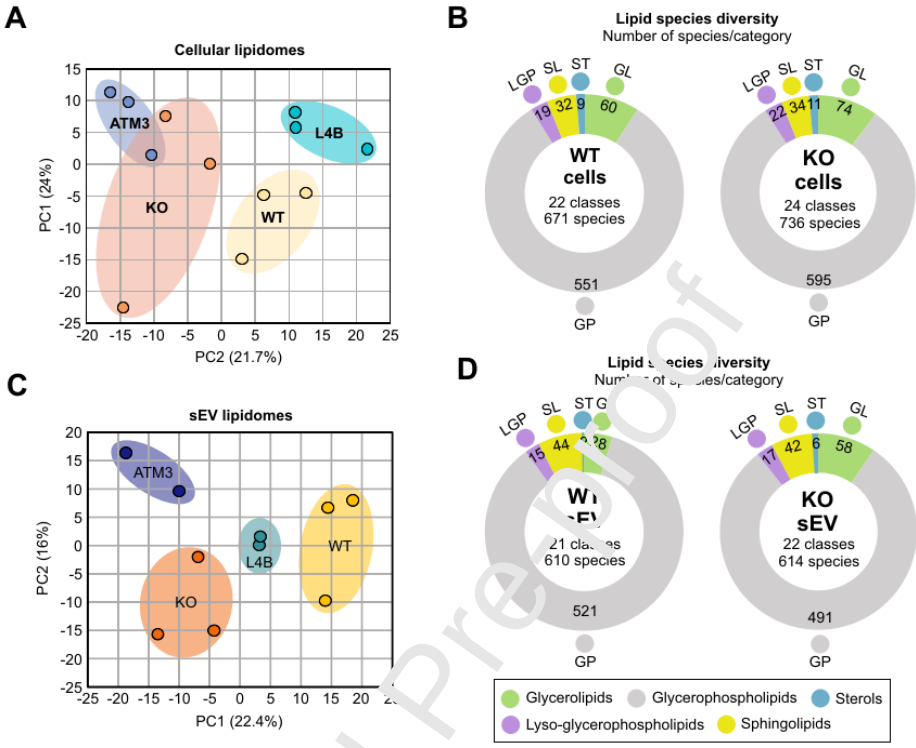

Fig. 3. Shotgun-lipidomic analysis of WT, KO, rescue L4B and mutant ATM3 sEVs and their parental cells. (A) PCA of cellular WT, KO, rescue L4B and mutant ATM3 lipidomes. Replicates of 3 independent experiments are shown. (B) Lipid class and species diversity among lipid categories is shown for cellular lipids in WT and KO cells. The numbers are the sum of unique lipids detected in at least one of the three replicates (n = 3 independent experiments). (C) PCA of sEVs in WT, KO, rescue L4B and mutant ATM3 lipidomes. Replicates of 2-3 independent experiments are shown. (D) Lipid class and species diversity (total number of species detected) among lipid categories is shown for sEVs released by WT and KO cells (n = 2-3 independent experiments).

3.5. Lipid profiles of cells and sEVs and the regulatory effect of LAPTM4B

A comprehensive lipidomic analysis showed that the lipid profile of sEVs substantially differed from that of their parental cells (**Supp. table 1**). Compared to cells, the sEVs were particularly enriched in phosphatidylserine (PS; 2.95x), cholesterol (Chol; 1.34x), sphingomyelin (SM; 1.3x), and ceramide (Cer; 1.85x) (**Supp. table 1**), similarly to what has been previously reported [4]. Storage lipids, such as triacylglycerol (TG) and cholesterol esters (CE) were virtually absent from sEVs, verifying the purity of our EV preparations (**Supp. table 1**).

Comparison of the lipid classes in WT vs KO cells revealed statistically significant, but quantitatively minor, changes in PE O-, SM, LPE O- and LPE (**Fig. 4A**). The effect of LAPTM4B was more obvious on the lipid classes detected in sEVs (**Fig. 4B**). In sEVs, total PS was reduced by 15% and total HexCers increased by 28%, suggesting that LAPTM4B preferentially regulates the secretion of these lipid classes.

Considering that several recent studies have provided evidence for a role of the LAPTM-family of proteins in sphingolipid metabolism [21,55–57], we next performed a detailed analysis of the individual sphingolipid species (**Fig. 5; Supp. Fig. 5**). Overall, the most abundant sphingolipid species present in A431 cells contained either C16 or C24 fatty acid moieties on the sphingoid backbone (**Fig. 5; Supp. Fig. 5**).

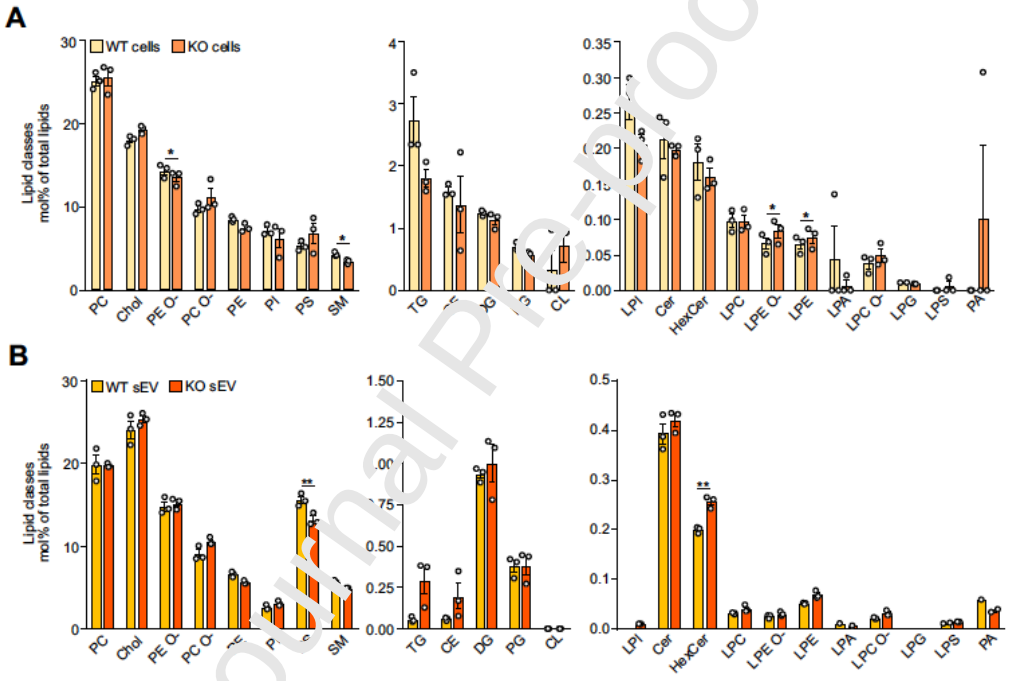

Fig. 4. Lipid class composition of WT and LAPTM4B knockout cells and sEVs. (A) Concentrations of lipid classes of WT and KO cells are shown in mol% of total lipids (n = 3 independent experiments; mean ± SEM). (B) Concentrations of lipid classes of WT and KO sEVs are shown in mol% of total lipids (n = 3 independent experiments; mean ± SEM). CE, cholesterol ester; Cer, ceramide; Chol, cholesterol; CL, cardiolipin; DG, diacylglyerol; HexCer, hexosylceramide; PA, phosphatidic acid; PC, phosphatidylcholine; PE, phosphatidylethanolamine; PG, phosphatidylglycerol; PI, phosphatidylinositol; PS, phosphatidylserine; and their respective lysospecies LPA; LPC; LPE; LPG; LPI; LPS; and their ether derivates: PC O-; LPC O-; PE O-; LPE O-; SM, sphingomyelin; TG, triacylglycerol. *p≤0.05; ** p≤0.005.

SM represented the most stable class of SLs in cells and sEVs, and LAPTM4B had only a moderate effect on certain species within this class (**Supp. Fig. 5**). LAPTM4B KO resulted in

an increase in C16 and C24 ceramide species primarily in cells and to a smaller extent in sEVs (**Fig. 5A - B**), confirming our previous findings with siRNA-mediated silencing of LAPTM4B [21]. Interestingly, LAPTM4B depletion resulted in a downregulation of deoxy-Cer42:2;1 (**Fig. 5A**), an atypical ceramide species generated via an alternative ceramide synthesis pathway in cells. The most striking LAPTM4B-dependent change in cells and sEVs was a marked increase of all HexCer species (**Fig. 5C - E**). Importantly, L4B but not ATM3 rescued the HexCer-accumulating phenotype, indicating a clear functional role of the SLim (**Fig. 5C - D**).

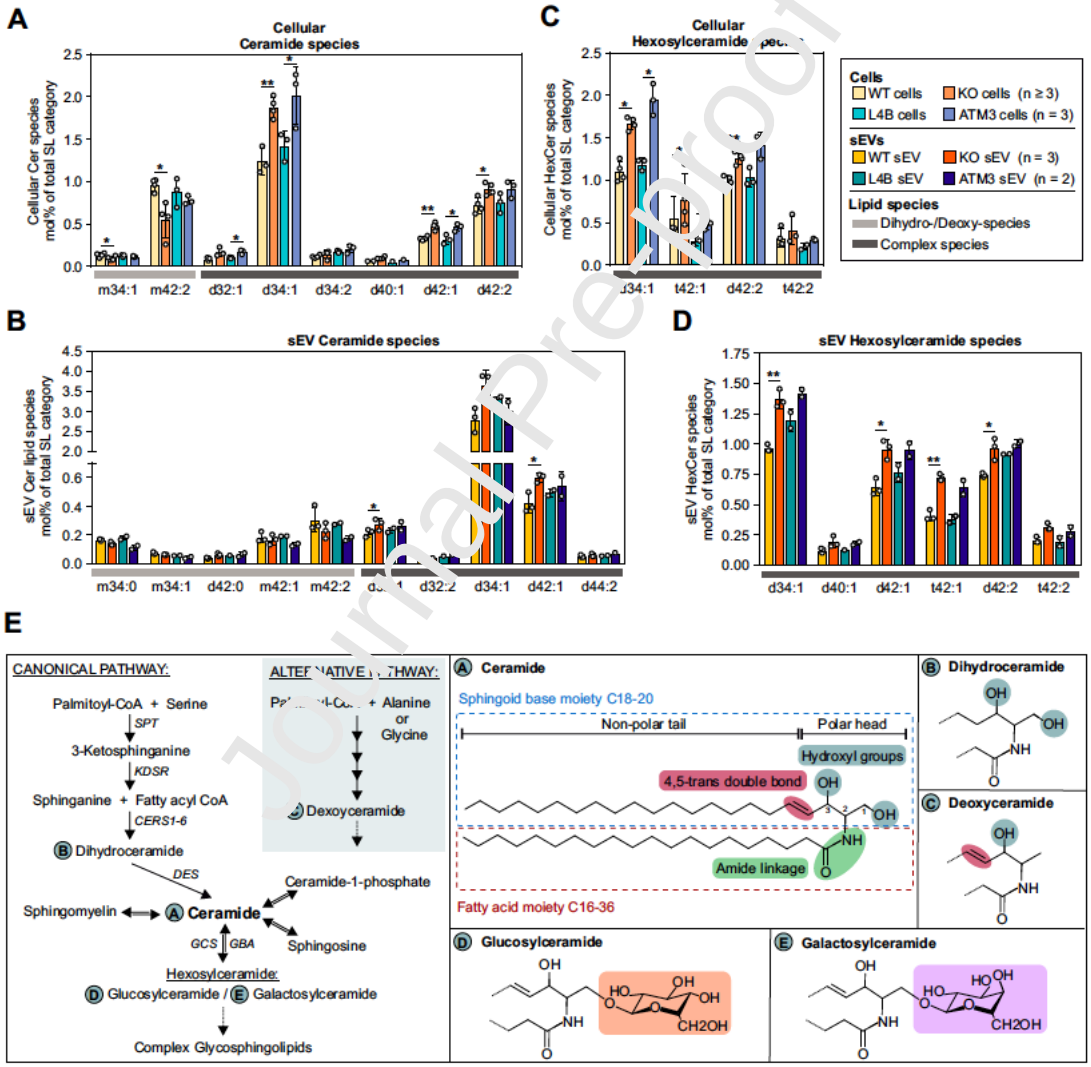

Fig. 5. LAPTM4B regulates the sphingolipid content of cells and sEVs. (A) Concentration of the most abundant Cer species detected in WT, KO, rescue L4B and mutant ATM3 cells are shown in mol% of total lipids. (n ≥ 3 independent experiments; mean ± SEM). (B) Concentration of the most abundant Cer species detected in WT, KO, rescue L4B and mutant ATM3 sEVs are shown in mol% of total lipids. (n = 3 independent experiments for WT and KO; n = 2 independent experiments for L4B and ATM3; mean ± SEM). (C) Concentration of the most abundant HexCer species detected in WT, KO, rescue

L4B and mutant ATM3 cells are shown in mol% of total lipids. (n ≥ 3 independent experiments; mean ± SEM). (D) Concentration of the most abundant HexCer species detected in WT, KO, rescue L4B and mutant ATM3 sEVs are shown in mol% of total lipids. (n = 3 independent experiments for WT and KO; n = 2 independent experiments for L4B and ATM3; mean ± SEM). (E) Schematic representation of sphingolipid synthesis pathways. Canonical and alternative SL synthesis in mammalian cells is depicted. SPT, serine palmitoyl-transferase; KDSR, 3-Ketosphinganine reductase; CERS1-6, ceramide synthases 1-6; DES, desaturase; GCS, glucosylceramide synthase; GBA, glucosylceramidase beta. Chemical structures of the SL metabolites, ceramide (A), Dihydroceramide (B), Deoxyceramide (C), Glucosylceramide (D), and Galactosylceramide (E) are shown. *p≤0.05; ** p≤0.005.

Knockout of LAPTM4A, another LAPTM family member, was recently found to inhibit cellular synthesis of Gb3, a downstream metabolite of HexCer, thereby protecting cells from enterohemorrhagic *Escherichia coli* (EHEC) infection [53–57]. Since Gb3 was not detected by the shotgun lipidomics approach, we performed [^{3}H]-sphingosine incorporation experiments to test whether LAPTM4B affects metabolites downstream of HexCer. These revealed that Gb3 levels were increased in LAPTM4B knockout cells, suggesting that LAPTM4A and LAPTM4B have opposing effects on cellular Gb3 (**Supp. Fig. 6**). Due to the low yield of radiolabeled sphingolipids in the sEV fraction we could not establish whether the Gb3 levels were altered in this fraction. Together, these data reveal a new role of LAPTM4B as potent regulator of sphingolipid content in the cell and in sEVs.

Another intriguing finding was a significant SLim-dependent co-regulation of ether-linked phospholipids (**Fig. 6**). By comparing WT and rescue L4B with KO and mutant ATM3, we observed a significant and SLim-dependent increase of certain ether-PC species and a concomitant reduction of ether-PE species in LAPTM4B-deficient cells (**Fig. 6A**). In sEVs, released by the afore mentioned cell lines, an opposite regulation was observed (**Fig. 6B**), with a reduction of ether-PC species, and an increase in ether-PE species. In particular, ether-PE species containing polyunsaturated fatty acids, including arachidonic acid (AA), docosapentaenoic (DPA) and docosahexaenoic acid (DHA), were enriched up to three-fold in sEVs from LAPTM4B-deficient cells. These results reveal that LAPTM4B-controlled modulation of sphingolipids is accompanied by a co-regulation of defined ether lipids.

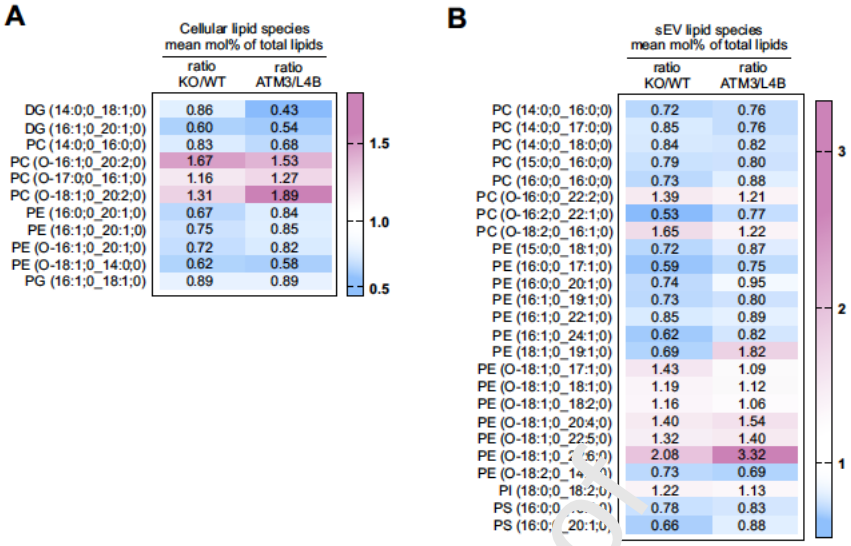

Fig. 6. LAPTM4B-SLim-dependent modulation of ester and ether lipid species in cells and sEVs. (A) Changes of cellular ester and ether lipid species from WT to KO and rescue L4B to mutant ATM3 cells are shown as ratios of their mean mol% values. All species listed are significantly regulated by the SLim in LAPTM4B (n=3). (B) Changes of sEVs ester and ether lipid species from WT to KO and rescue L4B to mutant ATM3 cells are shown as ratios of their mean mol% values. The species listed are significantly affected by LAPTM4B KO (n=3), and the phenotype is reversed by reintroduction of WT LAPTM4B but not by the SLim deficient mutant into KO cells (n=2).

3.6. LAPTM4B controls membrane order of sEVs

Together with ceramide and cholesterol, glycosphingolipids have been shown to drive lipid nanodomain formation in biological membranes, thereby effecting membrane properties [58]. Therefore, we tested whether LAPTM4B might control membrane order in sEVs. We used *trans*-parinaric acid (tPA), currently one of the most-sensitive probes to measure membrane order in biological membranes [59]. So far, tPA has been solely used to investigate membrane order in artificial membrane systems, such as liposomes [60]. Here, we used this probe to measure the order and the formation of nanodomains in membranes of cell-derived sEVs. The temperature-dependent average lifetime of the probe was used as a readout for measuring membrane order. The probe reported a similar average tPA lifetime for WT and KO sEVs membranes with a slight tendency of increased membrane order in KO sEVs (**Fig. 7A**).

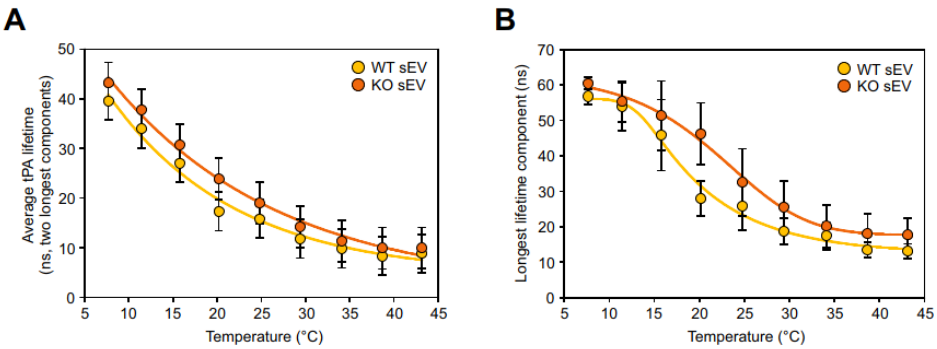

Figure 7. LAPTM4B effects the stability of membrane nanodomains in sEVs. (A) Membrane order and (B) nanodomain stability of sEVs membranes was measured by time-resolved fluorescence analysis using trans-parinaric acid (tPA) (n = 3 independent experiments, mean ± SEM).

Interestingly, measurement of the longest lifetime component (representing the smallest detectable domains) [58] suggested that sEVs secreted from KO cells had more stable nanodomains compared to WT sEVs (**Fig. 7B**). These data suggest that LAPTM4B regulates not only the lipid content but also membrane order of sEVs.

4. Discussion

Exosomes acquire their lipid composition during their biogenesis in MVEs. While many studies have addressed the mechanisms of protein sorting into ILVs [61], the factors controlling ILV/exosomal lipid content remain largely unknown. In the present study, we report a role for LAPTM4B in regulating the EV lipid composition.

Previous studies show that overexpressed LAPTM4B localizes to late endosomes or lysosomes based on colocalization with the markers CD63 or LAMP1. Our current findings suggest that endogenous LAPTM4B colocalizes partially with classical late endosomal/lysosomal protein markers, but particularly well with LBPA. This atypical phospholipid is enriched in highly specialized internal membranes of late endosomal compartments that function in protein sorting and trafficking [62] as well as in lipid degradation [63] and exosome biogenesis [48]. Immuno-EM shows that the vast majority of LAPTM4B is present in ILVs of MVEs. Accordingly, we find that LAPTM4B is secreted from human cells in sEVs both *in vitro* and *in vivo*. For the mechanistic studies of LAPTM4B regulation of EV lipid composition, we used the A431 cell model that has previously been used in investigations of LAPTM4B [19,21] and that secretes sufficient amounts of sEVs for

lipidomic analyses. Studies in additional cell models will be needed to address the generality of the observed effects.

We have previously shown that LAPTM4B regulates the subcellular distribution of ceramide [21]. The intracellular site(s) of LAPTM4B action have not been fully resolved, but its dominant MVE localization suggests a function in late endosomal organelles harboring ceramide as a result of sphingolipid catabolism. Here we show that a mutant LAPTM4B lacking the SLim [19] is not efficiently sorted into ILVs and displays altered secretion dynamics compared to the WT protein. The role of the SLim in promoting LAPTM4B targeting to ILVs is particularly interesting with regards to the reported role of ceramide in ILV formation [9,64]. Interestingly, pharmacological inhibition or silencing of nSMase2 inhibits exosome secretion in human breast cancer cells [16], but does not affect the release of exosomes from PC-3 prostate cancer cells [17]. Thus, different MVE subpopulations may use distinct mechanisms for ILV/exosome biogenesis [12].

The ability of ceramide to laterally segregate into nanodomains and to induce negative membrane curvature suggests a potential role in inward budding of nascent ILVs [65]. The SLim in LAPTM4B might sequester ceramide within the bilayer and thereby promote its own vesiculation into ILV membranes. Although LAPTM4B knockout leads to an increase in cellular C16- and C24-ceramides, it does not induce quantitative changes in EV secretion, size distribution, morphology or ceramide content. This implies that while LAPTM4B requires a SLim for ILV targeting, ceramide does not require LAPTM4B for sorting into MVEs.

The most substantial effect of LAPTM4B knockout on the lipidome is an increase in HexCer species both in cells and in sEVs. We further show that the HexCer suppressing effect of LAPTM4B is dependent on an intact SLim. The finding that LAPTM4B controls glycosphingolipid homeostasis is interesting considering that LAPTM4A (paralog with 71% similarity to LAPTM4B), is known to control Gb3 synthesis [55–57]. The stimulatory effect of LAPTM4A on Gb3 synthesis requires an interaction between LAPTM4A and Gb3 synthase in the Golgi [57]. To our surprise, LAPTM4B has the opposite effect, and suppresses cellular Gb3 levels. The study by Tian et al shows that both LAPTM4A and LAPTM4B interact with Gb3 synthase, but only LAPTM4A has a stimulatory effect on Gb3 synthesis [55]. Thus, the increased Gb3 synthesis in LAPTM4B knockout cells might result from enhanced LAPTM4A interaction with Gb3 synthase in the absence of the competing paralog. We show here that LAPTM4B localizes prominently to MVEs but it is plausible that it also functions in the Golgi to maintain glycosphingolipid homeostasis.

Another intriguing finding is the LAPTM4B SLim-dependent regulation of ether-PC and ether-PE species. Ether phospholipids are present in exosomes secreted from certain cell types, including platelets, PC-3 cells and mast cells [66]. Ether PLs have different physico-chemical properties compared to ester-PLs, and can pack into dense and rigid membrane structures [67], with proposed roles in regulating membrane trafficking and fusion [68]. Recently, Jiménez-Rojo and colleagues reported on a coordinated regulation of cellular ether lipids and sphingolipids, where a depletion of one class resulted in an increase in the other [69]. In LAPTM4B knockout cells, increased HexCers were coupled with a decrease in distinct ether PEs, while in LAPTM4B knockout sEVs, elevated HexCers were paralleled by increased PUFA-containing ether-PEs. The most enriched ether-PE species in sEVs, PE O-0/18:1;0_22:6:0, was present in sEVs, but not detected in cells. Notably, PUFA-containing phospholipids serve as precursors for the synthesis of lipid signaling molecules such as eicosanoids [70], and ether lipids and their fatty acids feed into eicosanoid production [71]. Finally, LAPTM4B deficiency led to more stable nanodomains in sEVs, in consistence with the observed increase in nanodomain-associated ether- and sphingolipids in sEVs. Changes in membrane order can affect e.g. vesicle stability and uptake by recipient cells [72–74], and the effect of LAPTM4B on EV functional properties should be addressed in future studies.

5. Conclusion

The LAPTM4 family of proteins are emerging as regulators of sphingolipid homeostasis, and we have previously shown that LAPTM4B regulates the subcellular distribution of ceramide [21]. The current study reveals that the impact of LAPTM4B goes beyond regulating a single lipid class. Rather, LAPTM4B controls the content of sphingolipids as well as co-modulates PUFA-containing ether lipids in cells and sEVs. This suggests that LAPTM4B may affect inflammatory properties of EVs. Considering that LAPTM4B associates with immune responses [75] and is linked to diseases associated with inflammatory signaling (e.g. several type of cancers [76–78]) and Lewy body dementia [79], an interesting avenue for future studies would be to address how LAPTM4B affects EV-mediated cell to cell signaling.

Author contributions

A.D., T.B., K.Z. designed the study. A.D. and T.B. supervised the study. A.D., K.Z., N.B., T.N., A.B., carried out the experiments. A.D., T.B., K.Z., N.B., T.N., A.B., P.M. analysed the data. A.D. wrote the first draft of the manuscript with input from all authors.

CRediT authorship contribution statement

Andrea Dichlberger: Conceptualization, Methodology, Validation, Formal analysis, Investigation, Resources, Writing – Original Draft, Review & Editing, Visualization, Supervision, Project administration. **Kecheng Zhou:** Methodology, Formal analysis, Investigation, Writing – Review & Editing, Project administration. **Nils Bäck**, **Thomas Nyholm, Anders Backman**: Methodology, Formal analysis, Investigation, Writing – Review & Editing. **Peter Matjus**: Supervision, Funding acquisition, Writing – Review & Editing. **Elina Ikonen:** Writing – Review & Editing, Supervision, Funding acquisition. **Tomas Blom**: Conceptualization, Methodology, Validation, Investigation, Formal analysis, Writing – Review & Editing, Supervision, Project administration Funding acquisition.

Acknowledgments

We thank Anna Uro and Josefin Halin for technical assistance. We thank the Extracellular Vesicle Core Facility at the University of Helsinki, Finland, for providing EV analytics services. We acknowledge the technical support by HiLIFE Light Microscopy platform and Biocenter Finland imaging infrastructure (Biomedicum Imaging Unit). We also thank the Electron Microscopy Unit of the institute of Biotechnology, University of Helsinki for providing laboratory facilities.

Funding

This work was supported by Academy of Finland (grants 303771 and 266092 to TB, 282192, 307415 and 312491 to EI), Sigrid Juselius Foundation (TB, EI), The Liv och Hälsa Foundation (TB), Finska Läkaresällskapet (NB), the Perklén Foundation (NB), and ILS doctoral programme of the University of Helsinki (KZ).

Declaration of interest statement

The authors report no conflict of interest.

Appendix A. Supplementary data

References

[1] G. van Niel, G. D'Angelo, G. Raposo, Shedding light on the cell biology of extracellular vesicles, Nat. Rev. Mol. Cell Biol. (2018). https://doi.org/10.1038/nrm.2017.125.

[2] M. Mathieu, L. Martin-Jaular, G. Lavieu, C. Théry, Specificities of secretion and uptake of exosomes and other extracellular vesicles for cell-to-cell communication, (n.d.). https://doi.org/10.1038/s41556-018-0250-9.

[3] M. Record, K. Carayon, M. Poirot, S. Silvente-Poirot, Exosomes as new vesicular lipid transporters involved in cell-cell communication and various pathophysiologies., Biochim. Biophys. Acta. 1841 (2014) 108–20. https://doi.org/10.1016/j.bbalip.2013.10.004.

[4] T. Skotland, K. Sandvig, A. Llorente, Lipids in exosomes: Current knowledge and the way forward, Prog. Lipid Res. (2017). https://doi.org/10.1016/j.plipres.2017.03.001.

[5] T. Skotland, K. Sagini, K. Sandvig, A. Llorente, An emerging focus on lipids in extracellular vesicles, Adv. Drug Deliv. Rev. (2020). https://doi.org/10.1016/J.ADDR.2020.03.002.

[6] S. Stuffers, C. Sem Wegner, H. Stenmark, A. Brech, Multivesicular Endosome Biogenesis in the Absence of ESCRTs, Traffic. 10 (2009) 925–937. https://doi.org/10.1111/j.1600-0854.2009.00920.x.

[7] M. Babst, MVB vesicle formation: ESCRT-dependent, ESCRT-independent and everything in between., Curr. Opin. Cell Biol. 23 (2011) 452–7. https://doi.org/10.1016/j.ceb.2011.04.008.

[8] F.X. Guix, R. Sannerud, F. Berditchevski, A.M. Arranz, K. Horré, A. Snellinx, A. Thathiah, T. Saido, T. Saito, S. Rajesh, M. Overduin, S. Kumar-Singh, E. Radaelli, N. Corthout, J. Colombelli, S. Tosi, S. Munck, I.H. Salas, W. Annaert, B. De Strooper, Tetraspanin 6: A pivotal protein of the multiple vesicular body determining exosome release and lysosomal degradation of amyloid precursor protein fragments, Mol. Neurodegener. (2017). https://doi.org/10.1186/s13024-017-0165-0.

[9] K. Trajkovic, C. Hsu, S. Chiantia, L. Rajendran, D. Wenzel, F. Wieland, P. Schwille, B. Brügger, M. Simons, Ceramide triggers budding of exosome vesicles into multivesicular endosomes., Science (80-.). 319 (2008) 1244–1247. https://doi.org/10.1126/science.1153124.

[10] G. van Niel, S. Charrin, S. Simoes, M. Romao, L. Rochin, P. Saftig, M.S. Marks, E. Rubinstein, G. Raposo, The tetraspanin CD63 regulates ESCRT-independent and -dependent endosomal sorting during melanogenesis., Dev. Cell. 21 (2011) 708–21. https://doi.org/10.1016/j.devcel.2011.08.019.

[11] E. Lauwers, Y.-C. Wang, R. Gallardo, R. Van der Kant, E. Michiels, J. Swerts, P. Baatsen, S.S. Zaiter, S.R. McAlpine, N. V. Gounko, F. Rousseau, J. Schymkowitz, P. Verstreken, Hsp90 Mediates Membrane Deformation and Exosome Release, Mol. Cell. 71 (2018) 689-702.e9. https://doi.org/10.1016/J.MOLCEL.2018.07.016.

[12] R. Ghossoub, F. Lembo, A. Rubio, C.B. Gaillard, J. Bouchet, N. Vitale, J. Slavík, M. Machala, P. Zimmermann, Syntenin-ALIX exosome biogenesis and budding into multivesicular bodies are controlled by ARF6 and PLD2, Nat. Commun. 5 (2014) 3477. https://doi.org/10.1038/ncomms4477.

[13] S. Phuyal, T. Skotland, N.P. Hessvik, H. Simolin, A. Øverbye, A. Brech, R.G. Parton, K. Ekroos, K. Sandvig, A. Llorente, The ether lipid precursor hexadecylglycerol stimulates the release and changes the composition of exosomes derived from PC-3 cells., J. Biol. Chem. 290 (2015) 4225–37. https://doi.org/10.1074/jbc.M114.593962.

[14] K. Yuyama, H. Sun, S. Mitsutake, Y. Igarashi, Sphingolipid-modulated exosome secretion promotes clearance of amyloid-β by microglia., J. Biol. Chem. 287 (2012) 10977–89. https://doi.org/10.1074/jbc.M111.324616.

[15] M.B. Dinkins, J. Enasko, C. Hernandez, G. Wang, J. Kong, I. Helwa, Y. Liu, A. V Terry, E. Bieberich, E. Bieberich, Neutral Sphingomyelinase-2 Deficiency Ameliorates

Alzheimer's Disease Pathology and Improves Cognition in the 5XFAD Mouse., J. Neurosci. 36 (2016) 8653–67. https://doi.org/10.1523/JNEUROSCI.1429-16.2016.

[16] K. Menck, C. Sönmezer, T.S. Worst, M. Schulz, G.H. Dihazi, F. Streit, G. Erdmann, S. Kling, M. Boutros, C. Binder, J.C. Gross, Neutral sphingomyelinases control extracellular vesicles budding from the plasma membrane., J. Extracell. Vesicles. 6 (2017) 1378056. https://doi.org/10.1080/20013078.2017.1378056.

[17] S. Phuyal, N.P. Hessvik, T. Skotland, K. Sandvig, A. Llorente, Regulation of exosome release by glycosphingolipids and flotillins, FEBS J. (2014). https://doi.org/10.1111/febs.12775.

[18] T. Skotland, K. Ekroos, D. Kauhanen, H. Simolin, T. Seierstad, V. Berge, K. Sandvig, A. Llorente, Molecular lipid species in urinary exosomes as potential prostate cancer biomarkers, Eur. J. Cancer. 70 (2017) 122–132. https://doi.org/10.1016/J.EJCA.2016.10.011.

[19] K. Zhou, A. Dichlberger, H. Martinez-Seara, T.K.M. Nyholm, S. Li, Y.A. Kim, I. Vattulainen, E. Ikonen, T. Blom, A Ceramide-Regulated Element in the Late Endosomal Protein LAPTM4B Controls Amino Acid Transporter Interaction., ACS Cent. Sci. 4 (2018) 548–558. https://doi.org/10.1021/acscentsci.7b00582.

[20] F.-X. Contreras, A.M. Ernst, P. Haberkant, P. Björkholm, E. Lindahl, B. Gönen, C. Tischer, A. Elofsson, G. von Heijne, C. Thiele, R. Pepperkok, F. Wieland, B. Brügger, Molecular recognition of a single sphingolipid species by a protein's transmembrane domain., Nature. 481 (2012) 525–9. https://doi.org/10.1038/nature10742.

[21] T. Blom, S. Li, A. Dichlberger, N. Bäck, Y.A. Kim, D. Loizides-Mangold, H. Riezman, R. Bittman, E. Ikonen, LAPTM4B facilitates late endosomal ceramide export to control cell death pathways., Nat. Chem. Biol. 11 (2015) 799–806. https://doi.org/10.1038/nchembio.1889.

[22] R. Milkereit, A. Persaud, L. Vanoaica, A. Guetg, F. Verrey, D. Rotin, LAPTM4b recruits the LAT1-4F2hc Leu transporter to lysosomes and promotes mTORC1 activation., Nat. Commun. 6 (2015) 7250. https://doi.org/10.1038/ncomms8250.

[23] S. Vergarajauregui, J. a Martina, R. Puertollano, LAPTMs regulate lysosomal function and interact with mucolipin 1: new clues for understanding mucolipidosis type IV., J. Cell Sci. 124 (2011) 459–68. https://doi.org/10.1242/jcs.076240.

[24] S. Hobbs, S. Jitrapakdee, J.C. Wallace, Development of a Bicistronic Vector Driven by the Human Polypeptide Chain Elongation Factor 1α Promoter for Creation of Stable Mammalian Cell Lines That Express Very High Levels of Recombinant Proteins, Biochem. Biophys. Res. Commun. 252 (1998) 368–372. https://doi.org/10.1006/BBRC.1998.9646.

[25] J.M. Falcón-Pérez, R. Nazarian, C. Sabatti, E.C. Dell'Angelica, Journal of Cell Science, J. Cell Sci. 110 (2005) 2227–2238. https://doi.org/10.1242/jcs.02633.

[26] J.-D. Pédelacq, S. Cabantous, T. Tran, T.C. Terwilliger, G.S. Waldo, Engineering and characterization of a superfolder green fluorescent protein, Nat. Biotechnol. 24 (2006) 79–88. https://doi.org/10.1038/nbt1172.

[27] V.T. Salo, S. Li, H. Vihinen, M. Hölttä-Vuori, A. Szkalisity, P. Horvath, I. Belevich, J. Peränen, C. Thiele, P. Somerharju, H. Zhao, A. Santinho, A.R. Thiam, E. Jokitalo, E. Ikonen, Seipin Facilitates Triglyceride Flow to Lipid Droplet and Counteracts Droplet Ripening via Endoplasmic Reticulum Contact, Dev. Cell. 50 (2019) 478-493.e9. https://doi.org/10.1016/J.DEVCEL.2019.05.016.

[28] J. Pinder, J. Salsman, G. Dellaire, Nuclear domain 'knock-in' screen for the evaluation and identification of small molecule enhancers of CRISPR-based genome editing, Nucleic Acids Res. 43 (2015) 9379. https://doi.org/10.1093/NAR/GKV993.

[29] I.W. McLean, P.K. Nakane, Periodate lysine paraformaldehyde fixative. A new fixative for immunoelectron microscopy, J. Histochem. Cytochem. 22 (1974) 1077–1083. https://doi.org/10.1177/22.12.1077.

[30] A. Salonen, L. Vasiljeva, A. Merits, J. Magden, E. Jokitalo, L. Kaariainen, Properly Folded Nonstructural Polyprotein Directs the Semliki Forest Virus Replication Complex to the Endosomal Compartment, J. Virol. 77 (2003) 1691–1702.

https://doi.org/10.1128/jvi.77.3.1691-1702.2003.
[31] E. Lázaro-Ibáñez, M. Neuvonen, M. Takatalo, U. Thanigai Arasu, C. Capasso, V. Cerullo, J.S. Rhim, K. Rilla, M. Yliperttula, P.R.M. Siljander, Metastatic state of parent cells influences the uptake and functionality of prostate cancer cell-derived extracellular vesicles, J. Extracell. Vesicles. (2017). https://doi.org/10.1080/20013078.2017.1354645.
[32] M.A. Livshts, E. Khomyakova, E.G. Evtushenko, V.N. Lazarev, N.A. Kulemin, S.E. Semina, E. V. Generozov, V.M. Govorun, Isolation of exosomes by differential centrifugation: Theoretical analysis of a commonly used protocol, Sci. Rep. (2015). https://doi.org/10.1038/srep17319.
[33] B.W. Sódar, Á. Kittel, K. Pálóczi, K. V. Vukman, X. Osteikoetxea, K. Szabó-Taylor, A. Németh, B. Sperlágh, T. Baranyai, Z. Giricz, Z. Wiener, L. Turiák, L. Drahos, É. Pállinger, K. Vékey, P. Ferdinandy, A. Falus, E.I. Buzás, Low-density lipoprotein mimics blood plasma-derived exosomes and microvesicles during isolation and detection, Sci. Rep. (2016). https://doi.org/10.1038/srep24316.
[34] Y. Yuana, J. Levels, A. Grootemaat, A. Sturk, R. Nieuwland, Co-isolation of extracellular vesicles and high-density lipoproteins using density gradient ultracentrifugation., J. Extracell. Vesicles. 3 (2014). https://doi.org/10.3402/jev.v3.23262.
[35] M. Puhka, M. Takatalo, M.-E. Nordberg, S. Valkonen, J. Nandania, M. Aatonen, M. Yliperttula, S. Laitinen, V. Velagapudi, T. Mirtti, C. Kallioniemi, A. Rannikko, P.R.-M. Siljander, T.M. Af Hällström, Metabolomic Profiling of Extracellular Vesicles and Alternative Normalization Methods Reveal Enriched Metabolites and Strategies to Study Prostate Cancer-Related Changes., Theranostics. 7 (2017) 3824–3841. https://doi.org/10.7150/thno.19890.
[36] R. Herzog, D. Schwudke, K. Schuhmann, J.L. Sampaio, S.R. Bornstein, M. Schroeder, A. Shevchenko, A novel informatics concept for high-throughput shotgun lipidomics based on the molecular fragmentation query language, Genome Biol. 12 (2011) R8. https://doi.org/10.1186/gb-2011-12-1-r8.
[37] C.S. Ejsing, J.L. Sampaio, V. Surendranath, E. Duchoslav, K. Ekroos, R.W. Klemm, K. Simons, A. Shevchenko, Global analysis of the yeast lipidome by quantitative shotgun mass spectrometry, Proc. Natl. Acad. Sci. U. S. A. 106 (2009) 2136–2141. https://doi.org/10.1073/pnas.0811700106.
[38] M.A. Surma, R. Herzog, A. Vasilj, C. Klose, N. Christinat, D. Morin-Rivron, K. Simons, M. Masoodi, J.L. Sampaio, An automated shotgun lipidomics platform for high throughput, comprehensive, and quantitative analysis of blood plasma intact lipids, Eur. J. Lipid Sci. Technol. 117 (2015) 1540–1549. https://doi.org/10.1002/ejlt.201500145.
[39] G. Liebisch, M. Binder, R. Schifferer, T. Langmann, B. Schulz, G. Schmitz, High throughput quantification of cholesterol and cholesteryl ester by electrospray ionization tandem mass spectrometry (ESI-MS/MS), Biochim. Biophys. Acta - Mol. Cell Biol. Lipids. 1761 (2006) 121–128. https://doi.org/10.1016/j.bbalip.2005.12.007.
[40] R. Herzog, K. Schuhmann, D. Schwudke, J.L. Sampaio, S.R. Bornstein, M. Schroeder, A. Shevchenko, LipidXplorer: A Software for Consensual Cross-Platform Lipidomics, PLoS One. 7 (2012) e29851. https://doi.org/10.1371/journal.pone.0029851.
[41] D. V. Kuklev, W.L. Smith, Synthesis of four isomers of parinaric acid, Chem. Phys. Lipids. 131 (2004) 215–222. https://doi.org/10.1016/j.chemphyslip.2004.06.001.
[42] L.A. Sklar, B.S. Hudson, R.D. Simoni, Conjugated Polyene Fatty Acids as Fluorescent Probes: Synthetic Phospholipid Membrane Studies, Biochemistry. 16 (1977) 819–828. https://doi.org/10.1021/bi00624a002.
[43] L.A. Sklar, B.S. Hudson, R.D. Simoni, Conjugated polyene fatty acids as fluorescent membrane probes: Model system studies, J. Supramol. Struct. 4 (1976) 449–465. https://doi.org/10.1002/jss.400040404.
[44] L.A. Sklar, B.S. Hudson, R.D. Simoni, Conjugated polyene fatty acids as membrane

probes: preliminary characterization, Proc. Natl. Acad. Sci. U. S. A. 72 (1975) 1649–1653. https://doi.org/10.1073/pnas.72.5.1649.
[45] T.K.M. Nyholm, D. Lindroos, B. Westerlund, J.P. Slotte, Construction of a DOPC/PSM/cholesterol phase diagram based on the fluorescence properties of trans -parinaric acid, Langmuir. 27 (2011) 8339–8350. https://doi.org/10.1021/la201427w.
[46] B.M. Castro, R.F.M. De Almeida, L.C. Silva, A. Fedorov, M. Prieto, Formation of ceramide/sphingomyelin gel domains in the presence of an unsaturated phospholipid: A quantitative multiprobe approach, Biophys. J. 93 (2007) 1639–1650. https://doi.org/10.1529/biophysj.107.107714.
[47] A.P.E. Backman, J. Halin, M.A. Kjellberg, P. Mattjus, Indirect Lipid Transfer Protein Activity Measurements Using Quantification of Glycosphingolipid Production, in: Methods Mol. Biol., 2019: pp. 105–114. https://doi.org/10.1007/978-1-4939-9136-5_9.
[48] J. Larios, V. Mercier, A. Roux, J. Gruenberg, ALIX- and ESCRT-III-dependent sorting of tetraspanins to exosomes., J. Cell Biol. 219 (2020). https://doi.org/10.1083/jcb.201904113.
[49] X. Tan, Y. Sun, N. Thapa, Y. Liao, A.C. Hedman, R.A. Anderson, LAPTM4B is a PtdIns(4,5)P2 effector that regulates EGFR signaling, lysosomal sorting, and degradation., EMBO J. 34 (2015) 475–90. https://doi.org/10.15252/embj.201489425.
[50] T. Blom, S. Li, A. Dichlberger, N. Bäck, Y.A.Y.A. Kim, U. Loizides-Mangold, H. Riezman, R. Bittman, E. Ikonen, LAPTM4B facilitates late endosomal ceramide export to control cell death pathways, Nat. Chem. Biol. 11 (2015) 799–806. https://doi.org/10.1038/nchembio.1889.
[51] S. Vergarajauregui, J.A. Martina, R. Puertollano, LAPTMs regulate lysosomal function and interact with mucolipin 1: new clues for understanding mucolipidosis type IV., J. Cell Sci. 124 (2011) 459–68. https://doi.org/10.1242/jcs.076240.
[52] J. Cerny, Y. Feng, A. Yu, K. Miyake, B. Borgonovo, J. Klumperman, J. Meldolesi, P.L. McNeil, T. Kirchhausen, The small chemical vacuolin-1 inhibits Ca2+-dependent lysosomal exocytosis but not cell resealing, EMBO Rep. 5 (2004) 883–888. https://doi.org/10.1038/sj.embor.7400243.
[53] K. Zhou, A. Dichlberger, E. Ikonen, T. Blom, Lysosome Associated Protein Transmembrane 4B (LAPTM4B)-24 Is the Predominant Protein Isoform in Human Tissues and Undergoes Rapid, Nutrient-Regulated Turnover, Am. J. Pathol. 190 (2020) 2018–2028. https://doi.org/10.1016/j.ajpath.2020.07.003.
[54] D.K. Jeppesen, A.M. Fenix, J.L. Franklin, J.N. Higginbotham, Q. Zhang, L.J. Zimmerman, D.C. Liebler, J. Ping, Q. Liu, R. Evans, W.H. Fissell, J.G. Patton, L.H. Rome, D.T. Burnette, R.J. Coffey, Reassessment of Exosome Composition, Cell. 177 (2019) 428-445.e18. https://doi.org/10.1016/J.CELL.2019.02.029.
[55] S. Tian, K. Muneeruddin, M.Y. Choi, L. Tao, R.H. Bhuiyan, Y. Ohmi, K. Furukawa, K. Furukawa, S. Boland, S.A. Shaffer, R.M. Adam, M. Dong, Genome-wide CRISPR screens for Shiga toxins and ricin reveal Golgi proteins critical for glycosylation, PLOS Biol. 16 (2018) e2006951. https://doi.org/10.1371/journal.pbio.2006951.
[56] T. Yamaji, T. Sekizuka, Y. Tachida, C. Sakuma, K. Morimoto, M. Kuroda, K. Hanada, A CRISPR Screen Identifies LAPTM4A and TM9SF Proteins as Glycolipid-Regulating Factors., IScience. 11 (2019) 409–424. https://doi.org/10.1016/j.isci.2018.12.039.
[57] A.R. Pacheco, J.E. Lazarus, B. Sit, S. Schmieder, W.I. Lencer, C.J. Blondel, J.G. Doench, B.M. Davis, M.K. Waldor, CRISPR Screen Reveals that EHEC's T3SS and Shiga Toxin Rely on Shared Host Factors for Infection., MBio. 9 (2018). https://doi.org/10.1128/mBio.01003-18.
[58] M. Cebecauer, M. Amaro, P. Jurkiewicz, M.J. Sarmento, R. Šachl, L. Cwiklik, M. Hof, Membrane Lipid Nanodomains, Chem. Rev. 118 (2018) 11259–11297. https://doi.org/10.1021/acs.chemrev.8b00322.
[59] O. Engberg, H.A. Scheidt, T.K.M. Nyholm, J.P. Slotte, D. Huster, Membrane Localization and Lipid Interactions of Common Lipid-Conjugated Fluorescence Probes, Langmuir. (2019) acs.langmuir.9b01202. https://doi.org/10.1021/acs.langmuir.9b01202.

[60] M.A. Al Sazzad, T. Yasuda, M. Murata, J.P. Slotte, The Long-Chain Sphingoid Base of Ceramides Determines Their Propensity for Lateral Segregation., Biophys. J. 112 (2017) 976–983. https://doi.org/10.1016/j.bpj.2017.01.016.
[61] T. Juan, M. Fürthauer, Biogenesis and function of ESCRT-dependent extracellular vesicles, Semin. Cell Dev. Biol. 74 (2018) 66–77. https://doi.org/10.1016/j.semcdb.2017.08.022.
[62] T. Kobayashi, E. Stang, K.S. Fang, P. de Moerloose, R.G. Parton, J. Gruenberg, A lipid associated with the antiphospholipid syndrome regulates endosome structure and function, Nature. 392 (1998) 193–197. https://doi.org/10.1038/32440.
[63] R. Sandhoff, K. Sandhoff, Emerging concepts of ganglioside metabolism, FEBS Lett. (2018). https://doi.org/10.1002/1873-3468.13114.
[64] A. Elsherbini, E. Bieberich, Ceramide and Exosomes: A Novel Target in Cancer Biology and Therapy., Adv. Cancer Res. 140 (2018) 121–154. https://doi.org/10.1016/bs.acr.2018.05.004.
[65] J.M. Holopainen, M.I. Angelova, P.K.J. Kinnunen, Vectorial budding of vesicles by asymmetrical enzymatic formation of ceramide in giant liposomes, Biophys. J. (2000). https://doi.org/10.1016/S0006-3495(00)76640-9.
[66] T. Skotland, N.P. Hessvik, K. Sandvig, A. Llorente, Exosomal lipid composition and the role of ether lipids and phosphoinositides in exosome biology., J. Lipid Res. 60 (2019) 9–18. https://doi.org/10.1194/jlr.R084343.
[67] T. Rog, A. Koivuniemi, The biophysical properties of ethanolamine plasmalogens revealed by atomistic molecular dynamics simulations., Biochim. Biophys. Acta. 1858 (2016) 97–103. https://doi.org/10.1016/j.bbamem.2015.10.023.
[68] N. Jiménez-Rojo, H. Riezman, On the road to unraveling the molecular functions of ether lipids., FEBS Lett. 593 (2019) 2378–2389. https://doi.org/10.1002/1873-3468.13465.
[69] N. Jiménez-Rojo, M.D. Leonetti, V. Zoni, A. Colom, S. Feng, N.R. Iyengar, S. Matile, A. Roux, S. Vanni, J.S. Weissman, H. Riezman, Conserved Functions of Ether Lipids and Sphingolipids in the Early Secretory Pathway, Curr. Biol. 30 (2020). https://doi.org/10.1016/j.cub.2020.07.059.
[70] V.D. Mouchlis, E.A. Dennis, Phospholipase A 2 catalysis and lipid mediator lipidomics, Biochim. Biophys. Acta - Mol. Cell Biol. Lipids. 1864 (2019) 766–771. https://doi.org/10.1016/j.bbalip.2018.08.010.
[71] D.I. Benjamin, A. Cozzo, X. Ji, L.S. Roberts, S.M. Louie, M.M. Mulvihill, K. Luo, D.K. Nomura, Ether lipid generating enzyme AGPS alters the balance of structural and signaling lipids to fuel cancer pathogenicity., Proc. Natl. Acad. Sci. U. S. A. 110 (2013) 14912–7. https://doi.org/10.1073/pnas.1310894110.
[72] J. Meldolesi, Exosomes and Ectosomes in Intercellular Communication, Curr. Biol. 28 (2018) R435–R444. https://doi.org/10.1016/j.cub.2018.01.059.
[73] E.R. Abels, X.O. Breakefield, Introduction to Extracellular Vesicles: Biogenesis, RNA Cargo Selection, Content, Release, and Uptake, Cell. Mol. Neurobiol. 36 (2016) 301–312. https://doi.org/10.1007/s10571-016-0366-z.
[74] S. Gill, R. Catchpole, P. Forterre, Extracellular membrane vesicles in the three domains of life and beyond, FEMS Microbiol. Rev. 43 (2019) 273–303. https://doi.org/10.1093/femsre/fuy042.
[75] C. Huygens, S. Liénart, O. Dedobbeleer, J. Stockis, E. Gauthy, P.G. Coulie, S. Lucas, Lysosomal-associated transmembrane protein 4B (LAPTM4B) decreases transforming growth factor β1 (TGF-β1) production in human regulatory T cells, J. Biol. Chem. 290 (2015) 20105–20116. https://doi.org/10.1074/jbc.M115.655340.
[76] Y. Li, L. Zou, Q. Li, B. Haibe-Kains, R. Tian, Y. Le, C. Desmedt, C. Sotiriou, Z. Szallasi, J.D. Iglehart, A.L. Richardson, Z.C. Wang, Amplification of LAPTM4B and YWHAZ contributes to chemotherapy resistance and recurrence of breast cancer, Nat. Med. 16 (2010) 214–218. https://doi.org/10.1038/nm.2090.
[77] Y. Meng, L. Wang, D. Chen, Y. Chang, M. Zhang, J.-J. XU, R. Zhou, Q.-Y. Zhang, LAPTM4B: an oncogene in various solid tumors and its functions, Oncogene. 35

(2016) 6359–6365. https://doi.org/10.1038/onc.2016.189.
[78] G.Z. Shao, R.L. Zhou, Q.Y. Zhang, Y. Zhang, J.J. Liu, J.A. Rui, X. Wei, D.X. Ye, Molecular cloning and characterization of LAPTM4B, a novel gene upregulated in hepatocellular carcinoma, Oncogene. 22 (2003) 5060–5069. https://doi.org/10.1038/sj.onc.1206832.
[79] C. Kun-Rodrigues, T. Orme, S. Carmona, D.G. Hernandez, O.A. Ross, J.D. Eicher, C. Shepherd, L. Parkkinen, L. Darwent, M.G. Heckman, S.W. Scholz, J.C. Troncoso, O. Pletnikova, T. Dawson, L. Rosenthal, O. Ansorge, J. Clarimon, A. Lleo, E. Morenas-Rodriguez, L. Clark, L.S. Honig, K. Marder, A. Lemstra, E. Rogaeva, P. St George-Hyslop, E. Londos, H. Zetterberg, I. Barber, A. Braae, K. Brown, K. Morgan, C. Troakes, S. Al-Sarraj, T. Lashley, J. Holton, Y. Compta, V. Van Deerlin, G.E. Serrano, T.G. Beach, S. Lesage, D. Galasko, E. Masliah, I. Santana, P. Pastor, M. Diez-Fairen, M. Aguilar, P.J. Tienari, L. Myllykangas, M. Oinas, T. Revesz, A. Lees, B.F. Boeve, R.C. Petersen, T.J. Ferman, V. Escott-Price, N. Graff-Radford, N.J. Cairns, J.C. Morris, S. Pickering-Brown, D. Mann, G.M. Halliday, J. Hardy, J.Q. Trojanowski, D.W. Dickson, A. Singleton, D.J. Stone, R. Guerreiro, J. Bras. A comprehensive screening of copy number variability in dementia with Lewy bodies., Neurobiol. Aging. 75 (2019) 223.e1-223.e10. https://doi.org/10.1016/j.neurobiolaging.2018.10.019.
[80] A.S. Chauhan, M. Kumar, S. Chaudhary, A. Dhiman, A. Patidar, P. Jakhar, P. Jaswal, K. Sharma, N. Sheokand, H. Malhotra, C.I. Raje, M. Raje, Trafficking of a multifunctional protein by endosomal microautophagy: linking two independent unconventional secretory pathways, FASEB J. 33 (2019) 5626–5640. https://doi.org/10.1096/fj.201802102R.

Credit Author Statement

Andrea Dichlberger: Conceptualization, Methodology, Validation, Formal analysis, Investigation, Resources, Writing – Original Draft, Review & Editing, Visualization, Supervision, Project administration. **Kecheng Zhou:** Methodology, Formal analysis, Investigation, Writing – Review & Editing, Project administration. **Nils Bäck**, **Thomas Nyholm, Anders Backman**: Methodology, Formal analysis, Investigation, Writing – Review & Editing. **Peter Matjus**: Supervision, Funding acquisition, Writing – Review & Editing. **Elina Ikonen:** Writing – Review & Editing, Supervision, Funding acquisition. **Tomas Blom**: Conceptualization, Methodology, Validation, Investigation, Formal analysis, Writing – Review & Editing, Supervision, Project administration Funding acquisition.

Declaration of competing interest

The authors declare that they have no known competing financial interests or personal relationships that could have appeared to influence the work reported in this paper.

Highlights

- A sphingolipid interaction motif regulates LAPTM4B sorting in endosomes.
- LAPTM4B is secreted from cells via extracellular vesicles *in vitro* and *in vivo*.
- The glycosphingolipid and ether lipid signature of extracellular vesicles is regulated by LAPTM4B.
- LAPTM4B modulates nanodomain formation in extracellular vesicle membranes.